

# Degeneracy-Aware Interpolation of 3D Diffusion Tensor Fields

Chongke Bi<sup>a</sup>, Shigeo Takahashi<sup>a</sup>, and Issei Fujishiro<sup>b</sup>

<sup>a</sup>The University of Tokyo, 5-1-5 Kashiwanoha, Kashiwa, Chiba 277-8561, Japan;

<sup>b</sup>Keio University, 3-14-1 Hiyoshi, Kohoku-ku, Yokohama 223-8522, Japan

## ABSTRACT

Visual analysis of 3D diffusion tensor fields has become an important topic especially in medical imaging for understanding microscopic structures and physical properties of biological tissues. However, it is still difficult to continuously track the underlying features from discrete tensor samples, due to the absence of appropriate interpolation schemes in the sense that we are able to handle possible degeneracy while fully respecting the smooth transition of tensor anisotropic features. This is because the degeneracy may cause rotational inconsistency of tensor anisotropy. This paper presents such an approach to interpolating 3D diffusion tensor fields. The primary idea behind our approach is to resolve the possible degeneracy through optimizing the rotational transformation between a pair of neighboring tensors by analyzing their associated eigenstructure, while the degeneracy can be identified by applying a minimum spanning tree-based clustering algorithm to the original tensor samples. Comparisons with existing interpolation schemes will be provided to demonstrate the advantages of our scheme, together with several results of tracking white matter fiber bundles in a human brain.

**Keywords:** Diffusion tensor fields, interpolation, degeneracy, eigenvalues and eigenvectors, minimum spanning trees.

## 1. INTRODUCTION

Visual analysis of 3D diffusion tensor fields has been widely employed for discovering the anisotropic behaviors in medical datasets by tracking characteristic biological tissues such as nerve and muscle fibers. This kind of visual analysis of diffusion tensor fields has been facilitated by the diffusion tensor magnetic resonance imaging (DT-MRI) technology especially for the purpose of medical diagnosis, where the distribution and motions of water molecules are measured as a grid of tensor samples in general. However, even with the latest DT-MRI devices, we still have a limited resolution along sagittal and coronal planes compared with the resolution obtained in axial planes. Interpolating over such discrete samples is a core integral part to visually analyze the continuous behaviors of anisotropic features inherent in the original 3D tensor fields.<sup>1</sup> Plausibly reconstructed tensor fields allow medical doctors to perform more sophisticated visual analysis, including *tractography*<sup>2</sup> and haptic rendering,<sup>3</sup> for more intuitive detection of structural anomalies.

Nonetheless, interpolating such 3D diffusion tensor fields is still a challenging task due to the following technical issues: (1) It is difficult to interpolate tensor fields consistently around *degenerate points*. This is because the degenerate points may cause rotational inconsistency of tensor anisotropy. (2) Special care must be taken to retain the anisotropic features inherent in the original dataset. In practice, these two problems have a close relationship, while existing techniques can resolve neither of these two or either of them at most. The technical difficulty lies in rigorously analyzing the topological structure of such tensor fields to properly locate possible degenerate points and then to explore smooth transition of tensor anisotropy. Our recent work<sup>4</sup> has tried to resolve these two problems in 2D tensor fields. First, we try to locate the possible *rotational inconsistency* around degenerate points using a *minimum spanning tree* (MST) strategy. Then, we rectify such rotational inconsistency by minimizing the rotational transformation locally. Finally, the eigenvectors and eigenvalues of the tensor samples will be separately interpolated. However, for fully understanding the microscopic structures of biological tissues in practice, an extension of this work to 3D tensor fields is necessary.

In order to extend the previous work to 3D diffusion tensor fields, we need to improve our approach so that we can resolve the above two technical problems by referring to the macroscopic structure of the original tensor field. This is because each tensor has much more neighbors in 3D diffusion tensor fields. For this reason, when constructing a minimum

---

Further author information: (Send correspondence to Chongke Bi)

Chongke Bi: E-mail: bichongke@visual.k.u-tokyo.ac.jp, Telephone: +81 4 7136 3957

Shigeo Takahashi: E-mail: takahashis@acm.org, Telephone: +81 4 7136 3956

Issei Fujishiro: E-mail: fuji@ics.keio.ac.jp, Telephone: +81 45 566 1752

spanning tree in 3D space, much more edges are left unconnected than in 2D space. This means that important edge may be omitted if we do not take good care of the distance metric of the MST. Furthermore, if the MST cannot extract the important edges, the number of *degenerate pairs* will increase. A large number of these degenerate pairs will increase our computation cost in the next phase where we rectify these degenerate pairs. Therefore, we will revise the MST distance metric in this paper. In the rectifying phase, in 2D case, we only minimize the rotational angle between the degenerate pairs, while we do not concern about the number of newly generated degenerate pairs. Nonetheless, in 3D case, we will define an objective function, which will be used to rectify degenerate pairs and decrease the number of newly generated degenerate pairs (cf. Section 4.3).

The rest of this paper is organized as follows: Section 2 provides a survey on related work in the fields of tensor interpolation and visualization. Section 3 explains eigenstructure-based representation of 3D diffusion tensors and related technical issues as the background knowledge for our proposed approach. Section 4 describes a minimum spanning tree-based algorithm for locating and resolving rotational inconsistency caused by degenerate points, which is followed by a scheme for interpolating 3D diffusion tensor fields in Section 5. Section 6 presents several experimental results to demonstrate the feasibility of the proposed scheme. Section 7 concludes this paper and refers to possible future extensions.

## 2. RELATED WORK

A 3D diffusion tensor is defined to be a symmetrical positive-definite  $3 \times 3$  matrix, or equivalently can be represented by an ellipsoid where the lengths of the three axes are the square roots of the three eigenvalues  $\lambda_1$ ,  $\lambda_2$ , and  $\lambda_3$  and its directions of the axes coincide with those of eigenvectors  $e_1$ ,  $e_2$ , and  $e_3$ . A *degenerate point* can be defined as at least two of the three eigenvalues are equal to each other.

The history of tensor interpolation methods started with component-wise linear interpolation of  $3 \times 3$  tensor matrices. Nonetheless, it cannot maximally retain the smooth transition of tensor anisotropy. Recently, Arsigny et al.<sup>5</sup> developed a new class of Riemannian metric called *log-Euclidean* to provide a faster computational algorithm, which transforms tensors into their matrix logarithms so that we can interpolate between them using Euclidean operations. However, their scheme still incurs unnecessary change in the anisotropy of the interpolated tensors. Kindlmann et al.<sup>6</sup> presented a novel tensor interpolation method called *geodesic-loxodrome*, which discriminates between the isotropic and anisotropic components of the tensors first and then interpolates each of the components individually. This accomplishes high quality interpolation results in the sense that it can maximally respect the smooth transition of tensor anisotropy, however, at the cost of longer computation time. The method may also incur undesirable discontinuity to the area around degenerate points.

Any of the aforementioned approaches tried to focus on tensor matrices, while less attention has been paid to the eigenstructures of the tensor matrices. Hotz et al. proposed a sophisticated model,<sup>7,8</sup> where they located degenerate points by linearly interpolating between each pair of eigenvalues and the corresponding pair of eigenvectors over the 2D triangulated domain using the component-wise method, respectively. However, extending their framework to 3D cases would be mathematically involved.

## 3. EIGENSTRUCTURE-BASED TENSOR REPRESENTATIONS

As described in the previous section, each diffusion tensor can be represented as an ellipsoid, and its degree of anisotropy effectively reflects the existence of the underlying fiber structures. Several metrics for evaluating such anisotropy have been proposed,<sup>9,10</sup> which include linearity ( $C_l$ ), planarity ( $C_p$ ), sphericity ( $C_s$ ), and Fractional Anisotropy ( $FA$ ).

For faithfully tracking characteristic fiber structures, we have to reconstruct the smooth transition of the anisotropy when interpolating tensors over the original data domain. In our approach, we resolve this problem by employing the eigenstructure of tensors so that we can directly manipulate the changes in the tensor anisotropy and orientation. Nonetheless, such interpolation schemes have not been fully tackled so far due to the following reasons. A tensor value has the sign ambiguity in eigenvector directions. This is because  $Ae_i = \lambda_i e_i$  and  $A(-e_i) = \lambda_i(-e_i)$  ( $i = 1, 2, 3$ ) hold simultaneously, where  $A$  represents the tensor matrix. Thus, we still have four different representations for a single tensor, even when we assume that the three eigenvalues suffice the condition  $\lambda_1 > \lambda_2 > \lambda_3 > 0$  and the associated normalized eigenvectors form a orthogonal right-handed coordinate system. Such sign ambiguity leads to multiple choices in making correspondences between two adjacent tensor samples.

When establishing the matching between the two set of eigenvectors, the existing methods implicitly assume that their eigenvectors are both sorted in descending order of their corresponding eigenvalues. However, this unexpectedly incurs

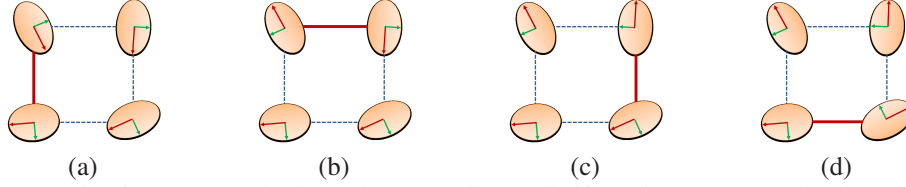


Figure 1: At least one pair of tensor samples has a large rotation angle if a unit square contains degeneracy. The red lines on the (a) left edge, (b) top edge, (c) right edge, and (d) bottom edge correspond to such pairs.

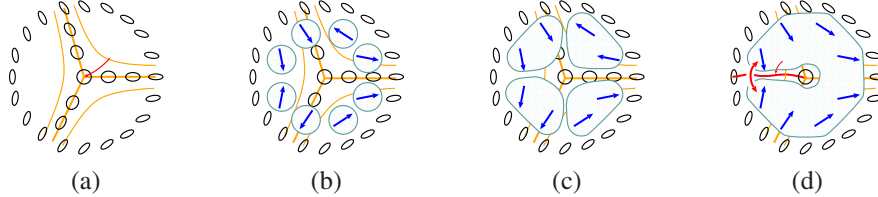


Figure 2: Locating a trisector degenerate point. (a) Tensor samples around the trisector degenerate point (indicated by the red arrow). (b) Clustering tensor samples into several small groups outlined in blue. (c) Merging small groups. (d) Clustering tensor samples into a single connected component while we find rotational inconsistency (indicated by the red arrows) along the red line emanating from the degenerate point.

another problem of tensor orientation alignment in the above eigenstructure-based representation, especially when the original tensor field contains degeneracy. This is because such degeneracy results in a cyclic path along which a large rotational angle between some pair of tensor samples is inevitable, as shown in Figure 1. This large rotational angle would cause redundant rotation on tensor anisotropic features.

In our approach, we resolve this problem by exhaustively searching for all the 24 possible correspondences between the two sets of eigenvalues and eigenvectors so that we can fully optimize the associated rotational transformation. The detail will be introduced in Section 4.3. A similar idea has been employed in the spectral analysis of data distribution,<sup>11</sup> while, to the best of our knowledge, this work is the first attempt to apply the idea to the interpolation of 3D diffusion tensors.

## 4. LOCATING TENSOR DEGENERACY

As described in Section 3, our proposed scheme generates smooth transition of tensor values by optimizing the correspondence around degenerate points. This suggests the need to locate possible degenerate points in the field first and then to rearrange the correspondence between eigenvalues/eigenvectors of several specific pairs of tensor samples when necessary.

### 4.1 Clustering tensor samples

According to Hesselink et al's study on tensor degeneracy,<sup>12</sup> tensor samples in the vicinity of a degenerate point become isotropic while the anisotropy becomes high if the corresponding samples are enough away from the degenerate point. This leads us to the idea of locating a degenerate point by identifying the smooth transition of high anisotropic tensors around it. For example, let us try to identify the position of a trisector, as shown in Figure 2(a). For seeking the smooth transitions of high anisotropic tensors, we employ a minimum spanning tree (MST) strategy to group discrete tensor samples if they share similar orientations and anisotropic features (Figure 2(b)). Here, we assume that the eigenvectors are arranged according to the descending order of the corresponding eigenvalues. We continue this clustering subprocess while we rearrange the directions of the tensor samples to be matched with each other if they fall into the same connected component (Figure 2(c)). This clustering subprocess terminates when we finish merging all the tensor samples into a single connected component. At this point, we can identify pairs of tensor samples that have redundant rotation, which illuminate the region of rotational inconsistency emanating from the degenerate point, as drawn in red in Figure 2(d).

For achieving this MST-based clustering of tensor samples, we evaluate the similarity between a pair of neighboring samples using the following distance metric, which has been obtained by extending the metric for 2D cases:<sup>4</sup>

$$d(D^S, D^T) = \alpha |C_l^S - C_l^T| + \beta |C_p^S - C_p^T| + \gamma (|\theta_1^{S,T}| / (\pi/2)) + \delta (|\theta_2^{S,T}| / (\pi/2)) + (|\lambda_1^S - \lambda_1^T| / (\lambda_1^{MAX} - \lambda_1^{MIN})), \quad (1)$$

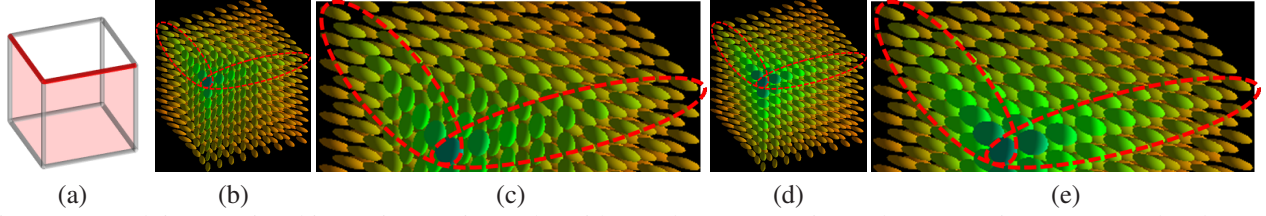


Figure 3: Resolving rotational inconsistency in a cube with two degenerate pairs (red segments in (a)). Interpolated tensor samples (b) before and (d) after the rotational inconsistency has been resolved, where (c) and (e) are the zoom-up views of the interpolated tensors around the two degenerate pairs in (b) and (d).

where the first, second and fourth terms, which are the same with the previous metric for 2D cases,<sup>4</sup> represent the difference of linearity, planarity and rotational angle between them. Note that  $\theta_2^{S,T}$  is the corresponding rotation angle between the right-handed coordinate systems defined by the two sets of eigenvector directions. The third and fifth terms have been newly introduced for 3D diffusion tensor fields. The third term is for the fibers in the brain, which are mainly affected by the primary eigenvectors of tensor samples.<sup>13</sup> The fifth term which evaluates the largest eigenvalue of the two tensor samples is used for differing the two tensors owing the same anisotropy and orientation but different sizes. This metric satisfies the fundamental axioms for metric spaces, and is used to evaluate the differences of the anisotropy between the two tensors together with the associated rotational angle. Our experiments suggest that  $\alpha = 60$ ,  $\beta = 10$ ,  $\gamma = 600$ , and  $\delta = 1$  are reasonable setting for this purpose.

## 4.2 Identifying pairs of rotational inconsistency

The region of rotational inconsistency that originates from a degenerate point will disturb the smooth transition of the interpolated results in later stage of the tensor interpolation as shown in Figures 3(b) and (c), which are the interpolated results from the cubic tensor field with two *degenerate pairs* represented by red segments in Figure 3(a). This is because the interpolated tensor samples have large rotations of their anisotropic features around that region. Our solution to this problem is to identify these degenerate pairs of tensor samples first, and then to optimize the rotational transformation associated with degenerate pairs by rearranging the correspondence between the two end samples for each pair. This naturally resolves the rotational inconsistency by introducing isotropic tensor samples, as shown in Figures 3(d) and (e).

In order to identify the degenerate pairs of tensor samples that incur large rotation angles, we first calculate the rotational transformation between the pair of adjacent samples that have not been connected by the MST network. We then label a pair as degenerate if the corresponding rotation angle is more than  $\pi/2$ .

After extracting all the degenerate pairs, we need to resolve the associated rotational inconsistency as shown in Figure 4. Here, we try to optimize a degenerate pair  $(D^S, D^T)$ , by rearranging the order of the eigenvectors of one end tensor sample, whose details will be provided in Section 4.3. However, this subprocess may cause new degeneracy at the other five edges that are incident to the modified tensor sample. Therefore, when we try to transform the degenerate pair  $(D^S, D^T)$  into a non-degenerate one, we should optimize the following five terms: (1) the rotational angle between their first eigenvector  $\theta_1^{S,T}$ ; (2) the rotational angle between the coordinate systems constituted by their eigenvectors  $\theta_2^{S,T}$ ; (3) the number of new degenerate pairs caused by this transformation  $n$ ; (4) the sum of the rotational angles between the first eigenvectors of the left five pairs  $\theta_1^{sum}$ ; (5) the sum of the rotational angles between the coordinate systems constituted by the eigenvectors of the left five pairs  $\theta_2^{sum}$ . For this purpose, we define an objective function  $f$  to evaluate the optimization subprocess.

$$f = a(\theta_1^{S,T}/\pi) + b(\theta_2^{S,T}/\pi) + c(n/6) + d(\theta_1^{sum}/(5\pi)) + (\theta_2^{sum}/(5\pi)), \quad (2)$$

where, the first two terms can be used to resolve the current pairs of rotational inconsistency, and the last three terms can be used to minimize the newly generated rotational inconsistency for improving the efficiency of our algorithm. Our experiments suggest that the parameter setting  $a = 4$ ,  $b = 2$ ,  $c = 2$ , and  $d = 2$  is reasonable for this optimization subprocess.

The subprocesses are shown in Figure 4. Suppose that we select one of the extracted degenerate pairs, as indicated by the red segment in Figure 4(a). Our first step is to select an unvisited tensor sample and optimize the associated rotation angle by choosing one of its 24 eigenstructure representations, as shown in Figure 4(b). If both of the two end tensor samples are unvisited, we select the more isotropic one of the two. Secondly, we check the number of newly generated

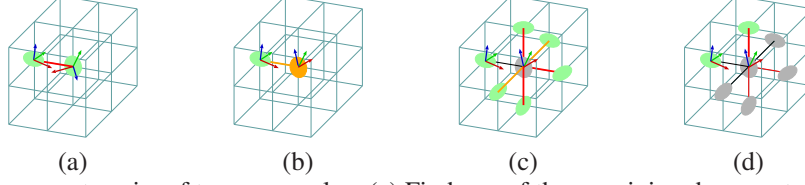


Figure 4: Resolving degenerate pairs of tensor samples: (a) Find one of the remaining degenerate pairs in red. (b) Rectify the degenerate pair into a non-degenerate one by transforming one end tensor sample (at the center). (c) Check the number of newly generated degenerate pairs (in red). (d) Continue this subprocess until all the degenerate pairs are resolved.



Figure 5: Configurations of degenerate pairs in a unit cube, where  $n$  is the number of degenerate pairs. A pair of tensor samples is drawn in red if it is degenerate, and a front (back) face is shaded in red (blue) if it contains a degenerate point.

degenerate pairs, which have been represented by red segments in Figure 4(c), while the yellow segments mean non-degenerate. Here, the first and second steps will be repeated to check all the 24 representations of the selected tensor sample for minimizing the objective function in Eq. (2), the details of which will be explained later. In this way, we can finally find one optimal representation of the selected tensor. We continue this optimizing subprocess by selecting another degenerate pair, as shown in Figure 4(d), until we transform all the degenerate pairs into non-degenerate ones. Here, we set a threshold of anisotropy to judge the degenerate pairs, because it is not necessary to consider the rotation angle between two isotropic tensors.

It should be noted here that the distribution of the degenerate pairs allows us to identify the existence of degenerate points over the original tensor field. In Figure 5, we list the configurations of degenerate pairs drawn in red lines. It is easy to see that the face in the unit cube contains a degenerate point (and thus shaded in red or blue) if it has an odd number of degenerate pairs because it contains redundant rotation of tensor anisotropy along its boundary cycle.

### 4.3 Resolving rotational inconsistency

Let us describe how we search all of the 24 possible correspondences between a pair of tensor samples to obtain their optimal correspondence. Suppose that we have two tensor samples  $D^S$  and  $D^T$ , and their normalized eigenvectors are represented as  $\{e_1^S, e_2^S, e_3^S\}$  and  $\{e_1^T, e_2^T, e_3^T\}$ , respectively. The rotation matrix  $R$  can be formulated as:

$$R = (p_{\sigma(1)}e_{\sigma(1)}^T, p_{\sigma(2)}e_{\sigma(2)}^T, p_{\sigma(3)}e_{\sigma(3)}^T)(e_1^S, e_2^S, e_3^S)^{-1}, \quad (3)$$

where  $\sigma(i)$  is a permutation of the index set  $\{1, 2, 3\}$  and  $p_i (i = 1, 2, 3)$  is defined to represent the sign ambiguity in the direction of each eigenvector  $e_i$ , in such a way that  $p_i = \pm 1 (i = 1, 2, 3)$  and  $\text{sgn}(\sigma)\prod_{i=1}^3 p_i = 1$ . Here,  $\text{sgn}(\sigma)$  denotes the signature of the permutation  $\sigma$ . The trace of  $R$  ( $\text{tr}R$ ) can be used to calculate the rotational angle  $\theta$  between  $D^S$  and  $D^T$  as:

$$\theta = \arccos |(\text{tr}R - 1)/2|. \quad (4)$$

## 5. INTERPOLATING 3D FIELDS OF DIFFUSION TENSORS

Having established the optimal correspondence between every pair of adjacent tensor samples, we can interpolate 3D tensor fields without any artifacts around degenerate points.

### 5.1 Interpolation using eigenvalues and eigenvectors

First of all, we consider how to interpolate two tensor samples in 1D as the simplest case. Suppose that we calculate the interpolated tensor  $D^M$  at the ratio of  $t : (1 - t)$  in the range  $[0, 1]$  between  $D^S$  ( $t = 0$ ) and  $D^T$  ( $t = 1$ ), as shown in Figure 6(a). We calculate the three eigenvalues  $\lambda_i^M (i = 1, 2, 3)$  of  $D^M$  by linearly interpolating the eigenvalues in  $D^S$  and  $D^T$ , and three eigenvectors  $e_i^M (i = 1, 2, 3)$  by linearly interpolating the associated rotation angle between them, as follows:

$$\lambda_i^M = t\lambda_i^S + (1 - t)\lambda_{\sigma(i)}^T \quad (5)$$

$$(e_{\sigma(1)}^M, e_{\sigma(2)}^M, e_{\sigma(3)}^M) = R^t(e_1^S, e_2^S, e_3^S) \quad (6)$$



Figure 6: Interpolating two diffusion tensor samples. The two sets of eigenvectors are (a) in the same orders and (b) in different orders.

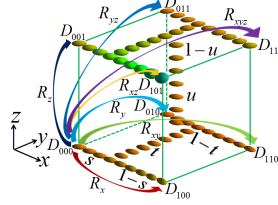


Figure 7: Interpolating a unit cube.

Here, the rotation matrix  $R$  is described in Eq. (3). Note that this formulation naturally allows us to introduce isotropic tensor values between the two tensor samples if the magnitudes of their eigenvalues have changed in their ordering. This effect is dominant when handling tensor samples in the neighborhood of a degenerate point as shown in Figure 6(b).

## 5.2 Combination of rotations for 3D domains

When interpolating between two tensor samples, the rotational transformation can be formulated in terms of a single value that parameterizes the interval between the samples. However, in 3D cases, the rotational transformation depends on three parameters  $s$ ,  $t$  and  $u$  that define the parameterization of the original data domain, and we have to deal with the order of applying the rotation matrices since they do not commute with one another in general.

In order to alleviate this non-commutative problem of matrix multiplication, we employ Alexa's formulation on linear combination of transformations.<sup>14</sup> Indeed, his formulation enables us to handle the multiplication of rotation matrices as their linear sum, and freely combine multiple rotational transformations without worrying about the order of composition. Suppose that we have a cube region confined by the discrete tensor samples  $D_{000}, D_{001}, D_{010}, D_{011}, D_{100}, D_{101}, D_{110}$ , and  $D_{111}$ , where the region is defined as a 3D parametric space  $(s, t, u) \in [0, 1] \times [0, 1] \times [0, 1]$ , as shown in Figure 7. If we denote Alexa's commutative multiplication operator by  $\oplus$ , we can calculate the rotational matrix that transforms  $D_{000}$  to the interpolated tensor at the parametric coordinates  $(s, t, u)$ , using the trilinear interpolation of matrices as follows:

$$R = R_x^{s(1-t)(1-u)} \oplus R_y^{(1-s)t(1-u)} \oplus R_z^{(1-s)(1-t)u} \oplus R_{xy}^{st(1-u)} \oplus R_{yz}^{(1-s)tu} \oplus R_{xz}^{s(1-t)u} \oplus R_{xyz}^{stu}, \quad (7)$$

where  $R_x, R_y, R_z, R_{xy}, R_{yz}, R_{xz}$ , and  $R_{xyz}$  correspond to the rotational transformations of  $D_{000}$  into  $D_{100}, D_{010}, D_{001}, D_{110}, D_{011}, D_{101}$ , and  $D_{111}$ , respectively. The tensor at  $(s, t, u)$  can be obtained by applying  $R$  to those of  $D_{000}$ .

## 6. RESULTS AND DISCUSSION

This section demonstrates the effectiveness of the present approach through the comparison with other existing interpolation schemes, followed by a discussion on the limitations of our scheme.

### 6.1 Results

Figures 8 and 9 show the results obtained from a human brain DT-MRI dataset. In order to demonstrate the effectiveness of our approach, we downsampled the original  $256 \times 256 \times 30$  DT-MRI data to  $128 \times 128 \times 15$ , and then applied the above interpolation schemes to extract the continuous behavior of the 3D diffusion tensor field. In the above strategy, the interpolated results using our scheme can track the underlying high anisotropic features even from the downsampled version of the DT-MRI dataset, and the result of our approach is better than those obtained by other existing schemes.

In Figure 8, we aim at tracking the fibers in the high anisotropic region from the seed point at the intersection of sagittal, coronal and axial planes. Figures 8(a), (b), and (c) are the interpolated results with the component-wise, log-Euclidean, and our schemes, respectively. Here, we track the fibers with  $C_l > 0.4$ . Note that the small windows at the lower left and

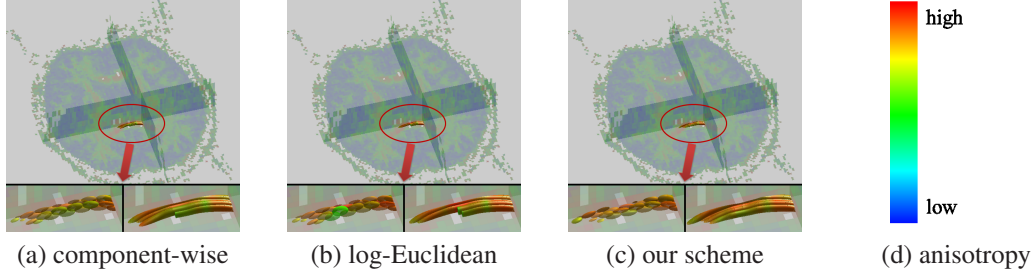


Figure 8: Tracking a fiber structure in a human brain DT-MRI dataset. The seed point is at the intersection of the sagittal, coronal and axial planes. Interpolated results with the (a) component-wise, (b) log-Euclidean, and (c) our schemes. (d) Color legend.

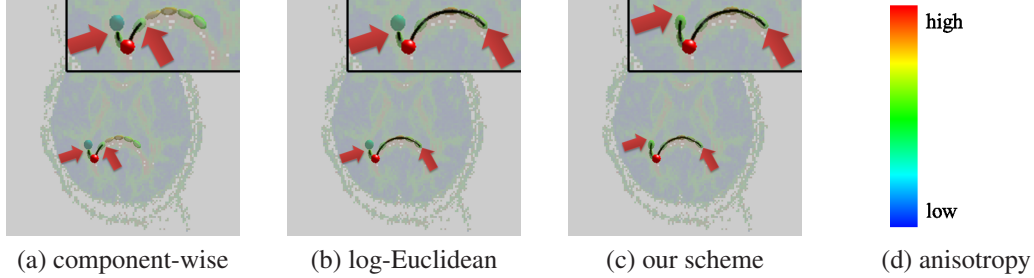


Figure 9: Tracking two fibers in a human brain DT-MRI dataset, where the red point is the seed point. Several degenerate points exist between the two fibers. Interpolated results with the (a) component-wise, (b) log-Euclidean, and (c) our schemes. The red arrows show the positions where the fiber tracking has terminated due to the interpolated tensors with low anisotropy. For clearly showing the results, the fibers have been represented by black curves. (d) Color legend.

lower right corners of the figures are the zoom-up views of the interpolated results, which are represented by ellipsoidal glyphs and fibers, respectively. Unfortunately, the fiber tracking subprocesses using the component-wise and log-Euclidean schemes stop on the highest point of the “arch bridge”-shaped fibers. This is because these two schemes cannot respect the anisotropic features when the rotational angle between the original tensor samples becomes larger. From the color of the interpolated tensors represented by ellipsoidal glyphs, we can see that the anisotropic features become lower. These low anisotropic tensor samples have been represented in green. On the other hand, our scheme can respect the anisotropic features of such kind of fibers, because the eigenvalues and eigenvectors are separately interpolated.

In Figure 9, we try to track the two fibers that are close to degeneracy in the tensor field, where the red point represents the seed point for tracking the two fibers. Figures 9(a), (b), and (c) are the interpolated results with the component-wise, log-Euclidean, and our schemes, respectively. The results have been visualized by ellipsoidal glyphs and fibers. Note that, for clearly showing the results, the fibers have been represented by black curves. Here, we track the fibers with  $C_l > 0.29$ . The positions at which the fiber tracking has terminated are indicated by the red arrows. Note that the small windows at the top-right corner are the zoom-up views of the interpolated results. The component-wise scheme cannot track the right fiber, and both the component-wise and the log-Euclidean schemes cannot track the left fiber due to the degeneracy in the region between the two fibers. Our scheme can fully track the two fibers, while avoiding the influence of existing degeneracy between the two fibers, as shown in Figure 9(c). This is because we successfully limit the size of the isotropic region while maximally respecting the anisotropy of the fibers.

## 6.2 Discussion

One of our concerns is the precision of the interpolated results especially in the neighborhood of degenerate points. Actually, the precision depends heavily on the density of the data sampling over the original diffusion tensor field. In our approach, we assume that we can extract only one degenerate point at most in a square face defined by four neighboring grid samples, and thus we cannot avoid generating spurious interpolated results when the face contains two or more degenerate points in reality. Furthermore, we can identify which square face contains a degenerate point while we cannot fully specify its accurate position within the face.

The smoothness of the original tensor field is another important factor to guarantee the plausibility of the interpolated results in our approach. This means that we cannot faithfully track the transition of the diffusion tensor values, when the original field contains sudden changes in tensor anisotropy and its orientation. This case indeed happens especially when the original data contains high-frequency noise.

## 7. CONCLUSION

This paper has presented an interpolation approach to visually analyzing the continuous behaviors of anisotropic features of 3D diffusion tensor fields. Our approach realizes a degeneracy-aware interpolation scheme in the sense that it aggressively locates the possible positions of tensor degeneracy. This has been accomplished by clustering tensor samples that share high anisotropic values and similar ellipsoidal representations using an MST strategy. Our scheme also analyzes the local topological structure of degenerate points to form degenerate lines, which can smooth the transition of anisotropic features. Several results are exhibited to demonstrate the feasibility of the present approach.

Our future extensions include visual analysis of the sophisticated interpolation results of the original tensor samples by employing higher-order interpolants. Our approach can also be applied to other applications, such as mesh generation, flow visualization, and so forth.

## ACKNOWLEDGMENTS

This work has been partially supported by JSPS under Grants-in-Aid for Scientific Research (B) No. 22300037, and challenging Exploratory Research No. 23650042 and No. 23650052.

## REFERENCES

- [1] Obermaier, H., Billen, M. I., Hagen, H., and Hering-Bertram, M., “Interactive visualization of scattered moment tensor data,” in [*Proceedings of SPIE 7868, 78680I*], (2011).
- [2] Muraki, S., Fujishiro, I., Suzuki, Y., and Takeshima, Y., “Diffusion-Based Tractography: Visualizing dense white matter connectivity from 3D tensor fields,” in [*Proceedings of Volume Graphics 2006*], 119–126 (2006).
- [3] Ogawa, Y., Fujishiro, I., Suzuki, Y., and Takeshima, Y., “Designing 6DOF haptic transfer functions for effective exploration of 3D diffusion tensor fields,” in [*Proceedings of World Haptics Conference 2009*], 470–475 (2009).
- [4] Bi, C., Takahashi, S., and Fujishiro, I., “Interpolating 3D diffusion tensors in 2D planar domain by locating degenerate lines,” in [*Proceedings of the 6th International Conference on Advances in Visual Computing*], Springer LNCS **6453**, 328–337 (2010).
- [5] Arsigny, V., Fillard, P., Pennec, X., and Ayache, N., “Log-Euclidean metrics for fast and simple calculus on diffusion tensors,” *Magnetic Resonance in Medicine* **56**(2), 411–421 (2006).
- [6] Kindlmann, G., Estepar, R., Niethammer, M., Haker, S., and Westin, C., “Geodesic-Loxodromes for diffusion tensor interpolation and difference measurement,” in [*Proceedings of Medical Image Computing and Computer-Assisted Intervention*], Springer LNCS **4791**, 1–9 (2007).
- [7] Hotz, I., Sreevalsan-Nair, J., and Hamann, B., “Tensor field reconstruction based on eigenvector and eigenvalue interpolation,” in [*Scientific Visualization: Advanced Concepts*], 110–123 (2010).
- [8] Sreevalsan-Nair, J., Auer, C., Hamann, B., and Hotz, I., “Eigenvector-based interpolation and segmentation of 2D tensor fields,” in [*Topological Methods in Data Analysis and Visualization*], 139–150 (2011).
- [9] Westin, C., Peled, S., Gudbjartsson, H., Kikinis, R., and Jolesz, F., “Geometrical diffusion measures for MRI from tensor basis analysis,” in [*Proceedings of International Society for Magnetic Resonance in Medicine*], 1742 (1997).
- [10] Pierpaoli, C. and Basser, P., “Toward a quantitative assessment of diffusion anisotropy,” *Magnetic Resonance in Medicine* **36**, 893–906 (2000).
- [11] Takahashi, S., Yoshida, K., Kwon, T., Lee, K. H., Lee, J., and Shin, S. Y., “Spectral-based group formation control,” *Computer Graphics Forum* **28**(2), 639–648 (2009).
- [12] Hesselink, L., Levy, Y., and Lavin, Y., “The topology of symmetric, second-order 3D tensor fields,” *IEEE Transactions on Visualization and Computer Graphics* **3**(1), 1–11 (1997).
- [13] Basser, P., Pajevic, S., Pierpaoli, C., Duda, J., and Aldroubi, A., “In vivo fiber tractography using DT-MRI data,” *Magnetic Resonance in Medicine* **44**(4), 625–632 (2000).
- [14] Alexa, M., “Linear combination of transformations,” *ACM Transactions on Graphics* **21**(3), 380–387 (2002).